Research Square

Preprints are preliminary reports that have not undergone peer review.
They should not be considered conclusive, used to inform clinical practice,
or referenced by the media as validated information.

Quantitative Characterization of Hydrogen Jet Stratification Using Combined PLIF-LIBS Diagnostics

Jungho Justin Kim
Korea Advanced Institute of Science and Technology
Seong-Young Lee
Michigan Technological University
Youngmin Ki
Korea Advanced Institute of Science and Technology
Heetae Yang
Korea Advanced Institute of Science and Technology
Munyoung Bae
Korea Advanced Institute of Science and Technology
Choongsik Bae
Korea Advanced Institute of Science and Technology
Joonsik Hwang
jhwang@kaist.ac.kr
Korea Advanced Institute of Science and Technology

Research Article

Keywords:

Posted Date: September 7th, 2026

DOI: https://doi.org/10.21203/rs.3.rs-10603159/v1

License: This work is licensed under a Creative Commons Attribution 4.0 International License.
Read Full License

Additional Declarations: No competing interests reported.

Abstract

Hydrogen direct injection offers high flame speed and zero-carbon operation, but its wide flammability requires precise control of mixture stratification. Optical diagnostics such as planar laser-induced fluorescence (PLIF) and laser-induced breakdown spectroscopy (LIBS) have been applied to study hydrogen jets. PLIF provided global visualization of hydrogen jet morphology, while LIBS supplied local equivalence-ratio measurements for calibration. By combining both techniques, quantitative two-dimensional fuel concentration fields of hydrogen jets were successfully reconstructed. Experiments in a constant-volume chamber at engine-like ambient pressure (0.5 MPa) and injection durations (500μs) demonstrated that the fused PLIF–LIBS approach quantified hydrogen jet stratification. Results revealed hollow-cone injection in the early stages, vortex-driven enrichment producing fuel-rich pockets in the mid stages, and momentum-dominated axial spreading in the later stages. The combined methodology overcomes the limitations of each diagnostic and provides a robust framework for validating CFD models and optimizing injection strategies for direct-injection hydrogen.

1 Introduction

Decarbonizing the transportation sector requires alternative fuels for applications where battery electrification remains difficult. While battery-electric vehicles are expanding rapidly in passenger transportation, their relatively low energy density limits their suitability for heavy-duty long-haul trucks, aviation, and maritime transport (White et al 2006). These sectors require energy carriers that can deliver large amounts of energy while maintaining a long operating range and reasonable refueling times.

Hydrogen has therefore received increasing attention as a potential carbon-free fuel. On a mass basis, hydrogen contains substantially more energy than conventional liquid fuels, with a gravimetric energy density of roughly 120 MJ/kg (White et al 2006). At the same time, its volumetric energy density is extremely low, even when stored at elevated pressures. Delivering sufficient fuel mass, therefore, requires injecting relatively large volumes of hydrogen, which typically produces high-momentum jets during fuel delivery. The interaction between the injected jet and the surrounding air determines how the mixture develops in space and time. Because ignition behavior, combustion stability, and pollutant formation are all sensitive to the local equivalence ratio, the way in which the hydrogen jet mixes with air becomes a central issue in hydrogen internal combustion engine (ICE) operation (Onorati et al 2022).

Hydrogen combustion also exhibits several characteristics that can enable efficient engine operation. Its wide flammability range and low ignition energy allow engines to operate under ultra-lean conditions, with excess-air ratios well above 2, thereby reducing nitrogen oxide emissions (Ji et al 2010). At the same time, these same properties can lead to challenges such as backfire and pre-ignition in premixed or port-fuel-injected systems (Goyal et al 2024; Park et al 2022; Sementa et al 2022). Direct injection (DI) offers a practical way to address these issues, as it suppresses backfiring, improves volumetric efficiency, and allows control of mixture stratification within the combustion chamber (Mohammadi et al

2007). Under such conditions, the transient development of the hydrogen jet plays a dominant role in determining the local mixture composition prior to ignition (Lee et al 2022).

For this reason, quantitative measurement of the equivalence-ratio field is an important step toward understanding hydrogen mixture formation. The spatial and temporal evolution of the mixture after the start of injection determines whether a flammable mixture is present near the ignition location and influences how the subsequent combustion process develops. Reliable measurements of this mixture field are therefore essential for interpreting the behavior of hydrogen combustion.

Optical diagnostic techniques have been widely used to investigate gaseous-fuel jet mixing (Zhao et al 2012). Planar laser-induced fluorescence (PLIF) using tracers such as acetone has been applied in many studies to visualize jet structure, penetration, and entrainment processes in gaseous jets (Kim et al 2025; Salazar 2009; Blotevogel et al 2004). PLIF provides spatially resolved and time-resolved images of mixture evolution, making it well-suited for observing jet dynamics. However, the measured fluorescence signal typically reflects relative concentration and must be calibrated to obtain quantitative information about the mixture. Conventional calibration approaches based on homogeneous reference mixtures or Raman measurements can be affected by fluctuations in laser energy, optical attenuation, and differences in diffusivity between the tracer and the fuel.

Laser-induced breakdown spectroscopy (LIBS), on the other hand, provides localized measurements of equivalence ratio through emission-ratio analysis (Ki et al 2025; Shudo et al 2009; Ki et al 2025). Because the measurement is based on atomic emission, LIBS is less sensitive to optical attenuation and laser-energy fluctuations and can provide accurate pointwise mixture information. Its main limitation is spatial coverage: LIBS measurements are inherently discrete and therefore cannot capture the transient two-dimensional structure of the mixing field.

In the present study, acetone-traced PLIF and LIBS are used together to obtain quantitative two-dimensional equivalence-ratio fields in a hydrogen jet under engine-relevant conditions. LIBS measurements are first used to determine the local equivalence ratio at selected locations within the jet, providing calibration points for the PLIF signal. The calibrated relationship is then used to convert PLIF intensity into quantitative equivalence-ratio fields through regression-based scaling. This combined approach enables observation of the transient development of hydrogen jet mixing over a wide field while maintaining quantitative accuracy. The resulting measurements provide detailed information on hydrogen jet mixture formation and offer useful experimental data for comparison with numerical simulations of hydrogen injection and combustion processes (Kazmouz et al 2021; Dee 2009; Smirnov et al 2014).

2 Experiment Setup

2.1 Combustion chamber and optics

Experiments were conducted in a 1.4 L constant-volume chamber (CVC) with four 100 mm optical windows, providing full optical access similar to configurations used in previous mixture-formation studies (Kim et al 2025; Blotevogel et al 2004). A PHINIA hollow-cone, outward-opening direct injector delivered hydrogen at 4 MPa, while the chamber was filled with nitrogen at 0.5 MPa to prevent unwanted ignition and mimic ambient pressure. An injection duration of 500 μs was selected to capture jet development during and after injection. The chamber geometry and conditions were chosen to replicate engine-relevant mixture formation of the compression stroke while maintaining optical clarity (Kim et al 2025; Ki et al 2025; Ki et al 2025). The details of the experiment setup are shown in Table 1. Laser timing was used to observe the behavior of the hydrogen jet during and after injection. The fuel and ambient temperatures were maintained at 288 K and 323 K, respectively. Figure 1 shows each timing on a single timeline starting from the start of injection.

To visualize hydrogen jet evolution, acetone was employed as a fluorescent tracer (≈ 0.2 mol%) premixed with hydrogen in a separated mixing chamber shown in Fig. 2, following prior PLIF validations (Salazar et al 2009; Blotevogel et al 2004). A 266 nm pulsed Nd:YAG laser was expanded into a thin sheet using a convex lens with a focal length of 1000 mm and a plano-concave cylindrical lens with a focal length of -25.4 mm that traversed the jet region. The laser beam excited acetone, which had an excitation wavelength between 225–320 nm, on the plane (Alfonso-Olmos et al 2025). The concentration of hydrogen was indirectly measured using the brightness of the excited acetone at the pixel. The resulting 325–500 nm fluorescence from acetone was recorded using an intensified high-speed camera (Phantom EVO710 and Lambert HiCAM). Twenty images per condition were captured to increase the repeatability of the gaseous fuel. Image-processing and normalization techniques, adapted from established methods (Blotevogel et al 2004), substantially enhanced signal quality and spatial resolution. These post-processed PLIF images provided a detailed, time-resolved visualization of global jet morphology. The detailed experiment setup of the PLIF measurement is shown in Fig. 3.

To obtain quantitative data, laser-induced breakdown spectroscopy (LIBS) was used for local calibration. A 532 nm high-energy laser pulse generated plasma emissions at selected locations, yielding spectra with hydrogen (656 nm) and nitrogen (871 nm) lines. Calibration curves were established using homogeneous H_2/N_2 mixtures of known composition, correlating the intensity of hydrogen with the intensity of nitrogen ratios (I_H/I_N) with equivalence ratio (Shudo et al 2009). Thirty LIBS measurements were averaged to improve repeatability. Schlieren images were recorded simultaneously to facilitate intuitive analysis of jet formation, although the video was not included in the results. The details of the LIBS experimental setup are shown in Fig. 3.

Finally, PLIF and LIBS were integrated into a unified calibration framework: twenty PLIF images captured at various jet-development times were normalized for laser fluctuations, while concurrent LIBS data provided absolute local equivalence ratios. Correlating these datasets produced a robust regression linking PLIF intensity to quantitative hydrogen concentration fields. This approach mitigated beam non-uniformity effects and enabled two-dimensional, time-resolved equivalence-ratio mapping suitable for CFD validation.

2.2 Experimental uncertainty

Uncertainty in the combined PLIF–LIBS approach arises from both diagnostic limitations and injection variability. For PLIF, major contributions include laser pulse-to-pulse energy fluctuations (typically ± 5%), mainly due to spatial non-uniformity of the laser sheet. Additional uncertainty stems from tracer–fuel diffusivity mismatch and cycle-to-cycle variation in injected hydrogen mass, which has been reported at the level of ~ 2% in constant-volume chamber experiments (Kim et al 2025; Ki et al 2025). Similar issues have been noted in previous acetone-PLIF studies, where intensity variations are strongly influenced by beam profiles and optical alignment (Salazar et al 2009; Blotevogel et al 2004).

For LIBS, the primary sources of uncertainty arise from sensitivity to the plasma formation threshold and local density fluctuations within the jet. By averaging thirty consecutive spectra at each calibration location, this scatter was reduced, yielding an estimated local equivalence ratio uncertainty of ± 0.05 (Shudo et al 2009). Combining ensemble-averaged PLIF images with regression-based LIBS calibration further mitigates shot-to-shot fluctuations, producing robust quantitative equivalence ratio maps. Based on error propagation from both diagnostics, the overall uncertainty of the reconstructed two-dimensional concentration fields is estimated to be within ± 10%.

In addition, hydrogen is a gaseous fuel, so jet shapes vary shot-by-shot, which means the average measurement is more unstable by ± 10%.

3 Results and Discussions

3.1 Calibration procedure

The combined PLIF–LIBS methodology used to obtain the quantitative equivalence ratio field is illustrated in Fig. 4. For each injection condition, a sequence of twenty raw acetone–PLIF images was first acquired (upper left). Each of these images was processed to extract the fluorescence intensity field by converting the raw signal into an intensity map and removing the background contribution (upper right). The intensity of the processed images represents the instantaneous spatial distribution of the tracer fluorescence associated with the hydrogen jet.

To reduce shot-to-shot variability and obtain a statistically stable representation of the jet structure, the twenty processed PLIF intensity images were ensemble-averaged, producing one mean fluorescence intensity field image (lower right).

In parallel with the PLIF measurements, LIBS measurements were performed at a fixed reference location within the jet. Multiple LIBS spectra from thirty measurements were acquired at the exact point to determine the local equivalence ratio based on the measured hydrogen and nitrogen emission signals. This LIBS-derived equivalence ratio serves as an absolute calibration reference.

Finally, the averaged PLIF intensity field was scaled using the LIBS reference value at the same spatial location of the hydrogen jet. Through this calibration step, the fluorescence intensity distribution was converted into a quantitative two-dimensional equivalence ratio map, as shown in the lower left of Fig. 4.

To achieve quantitative accuracy, the PLIF data were anchored using local LIBS measurements. A high-energy 532 nm laser pulse was focused within the jet to generate plasma, and reduce shot-to-shot fluctuations, thirty emission intensities of hydrogen and nitrogen were recorded for one condition. This reference value was then matched with the corresponding PLIF intensity at the same spatial point, establishing a calibration link between fluorescence intensity and absolute fuel concentration.

Once the calibration point was established, the correlation between the equivalence ratio and PLIF intensity was applied across the entire measurement domain, enabling conversion of relative PLIF intensity distributions into quantitative two-dimensional equivalence ratio maps.

The combination of the two diagnostics overcomes the inherent limitations of each individual technique. PLIF provides high-resolution two-dimensional spatial information, but achieving reliable absolute calibration of PLIF intensity alone requires complex procedures and is difficult to implement under practical experimental conditions. In contrast, LIBS provide quantitative equivalence ratio measurements but only at discrete spatial locations. By linking the local LIBS measurement to the PLIF intensity field, this combined diagnostic approach enables quantitative mapping of the equivalence ratio over the entire jet, providing a robust framework for investigating hydrogen jet stratification under engine-relevant conditions.

The calibration between LIBS-derived equivalence ratio and PLIF fluorescence intensity is presented in Fig. 5. Each symbol represents one calibration condition obtained by pairing the mean PLIF intensity at the LIBS reference location with the corresponding equivalence ratio measured by LIBS. The horizontal error bars indicate the uncertainty in PLIF fluorescence intensity, which reflects shot-to-shot variation in the PLIF signal, background-subtraction effects, and local spatial variability near the reference location. The vertical error bars indicate the uncertainty in the LIBS-derived equivalence ratio, arising from repeat LIBS measurements and the associated variability in the spectral signal used for concentration estimation.

A fourth-order polynomial was used to represent the calibration curve between fluorescence intensity and equivalence ratio. This form was selected because it provided sufficient flexibility to capture the strongly nonlinear increase in the equivalence ratio as PLIF intensity increased over the measured range while going through the origin. Passing through the origin is crucial for the calibration process to eliminate negative values of the equivalence ratio. The fourth-order polynomial was chosen over second- or third-order because it provided the lowest RMS while following the trendline. The fitted curve was constrained to remain physically meaningful within the calibration domain, such that the predicted equivalence ratio remained positive. The resulting quartic expression was then used to convert PLIF intensity into equivalence ratio for the construction of two-dimensional quantitative maps.

The figure also illustrates both the strengths and limitations of the calibration. A major advantage is that the fitted trend captures the overall monotonic increase between fluorescence intensity and equivalence ratio, enabling practical conversion of spatially resolved PLIF data into quantitative mixture fields. At the same time, the presence of both horizontal and vertical error bars indicates that uncertainty exists in both diagnostics: PLIF introduces uncertainty in the measured intensity, while LIBS introduces uncertainty in the local equivalence ratio. The uncertainty becomes more noticeable at a higher equivalence ratio, where the error bars widen, and the calibration points are more sparsely distributed. This indicates that the fitted curve is most reliable within the range directly supported by measurements, whereas extrapolation beyond that range should be interpreted with caution.

3.2 Hydrogen jet structure

After establishing the calibration between PLIF fluorescence intensity and equivalence ratio, the spatial and temporal evolution of the hydrogen jet can be examined. Figure 6 presents synchronized schlieren and PLIF images that capture the jet development following fuel injection. The total injection duration was 500 μs, allowing the jet formation to be observed both during the injection process and after the end of injection. By comparing the two measurements at the same delay times after the start of injection, the global jet evolution and the internal fuel distribution can be examined simultaneously, providing a clearer picture of hydrogen jet development.

Figure 6 shows the temporal evolution of the hydrogen jet following injection, visualized simultaneously by schlieren and PLIF measurements. The injection duration was 500 μs, allowing the jet development to be observed both during and after the injection event. Both diagnostics reveal the same large-scale jet growth and penetration as delay time increases, but they highlight different aspects of the underlying jet physics.

At the early stage (T_{SOI} = 200 μs), the schlieren image shows the initial expansion of the jet with a clear hollow-cone structure emerging from the injector. The PLIF map reveals that the fuel distribution is concentrated near the outer portions of the jet, forming two ribbon-like lobes, while the center region remains weak in intensity. This indicates that the injected hydrogen initially spreads outward along the nozzle opening direction, producing a hollow fuel distribution with a relatively lean core.

As the jet develops (T_{SOI} = 400–600 μs), the schlieren images show the forward propagation of the jet head and the roll-up of the leading edge, characteristic of a developing vortex structure. The PLIF maps show that this region corresponds to localized enrichment near the jet tip and along the central portion of the plume, where the equivalence ratio approaches $\Phi \approx 1$. This behavior indicates that the vortex motion at the jet head entrains and accumulates fuel, producing richer pockets near the front of the jet, while the trailing region becomes progressively leaner due to mixing with the ambient gas.

After the end of injection (T_{SOI} = 800 μs), the schlieren image shows an elongated jet plume continuing to propagate downstream, indicating that the jet momentum continues to drive the flow even after fuel delivery stops. In contrast, the PLIF map shows that the mixture field evolves differently: the highest

concentrations remain along the jet centerline, while the outer regions become increasingly diluted ($\Phi < 0.25$) due to strong entrainment of surrounding gas. This indicates that while the global jet structure continues to evolve under momentum-driven transport, the mixture distribution becomes progressively more stratified and diluted. In addition, the side plume near the injector tip shown in the schlieren image is not visible in the PLIF image. This is because the schlieren image shows the volumetric side view while the PLIF image is the cross-sectional view from the side. The plume is simply not located on the same plane where the PLIF image was taken.

The sequence reveals the dynamic evolution of hydrogen jet mixing. The injector geometry produces a hollow-cone structure during the earliest stage of injection, establishing a non-uniform fuel distribution near the nozzle. As the jet develops, vortex dynamics at the jet head promote local fuel accumulation and enrichment in the leading region of the plume. After the end of injection, axial momentum and entrainment dominate the plume evolution, leading to downstream spreading and progressive dilution of the mixture. These observations highlight a clear progression of jet physics—from geometry-driven initial spreading, to vortex-induced enrichment, and finally to momentum-driven dispersion.

3.3 Outer Opening Hollow-cone shaped Pinhole injector characteristics

The transient response of the pinhole injector during needle closure can produce small fluctuations in the injected mass flow. In particular, needle rebound and delayed hole closure may cause a brief secondary release of hydrogen after the nominal end of injection. The resulting mixture structures can be identified from the spatial and temporal evolution of the equivalence-ratio field.

Figure 7 shows the temporal evolution of the mixture field after the end of injection, presented as PLIF-derived equivalence-ratio maps together with the corresponding centerline profiles extracted along the jet axis. At T_{SOI} = 1100 μs, the PLIF map shows that the main hydrogen plume has already propagated downstream. The centerline profile confirms this behavior, exhibiting a broad peak around 40–50 mm downstream of the injector with an equivalence ratio of approximately $\Phi \approx 0.9$, indicating that the fuel from the primary injection event has formed an extended plume that is already undergoing mixing with the surrounding gas.

At T_{SOI} = 1200 μs, the PLIF structure remains similar, but the centerline profile shows a reduction and smoothing of the peak equivalence ratio, reflecting continued entrainment-driven dilution of the previously injected hydrogen as the jet momentum decays.

A markedly different behavior appears at T_{SOI} = 1250 μs. The PLIF image reveals a localized high-concentration region near the injector, located approximately 15–20 mm downstream of the nozzle. The centerline profile captures this event as a sharp upstream peak exceeding $\Phi \approx 1.3$, while the downstream portion remains relatively lean. The separation between the upstream peak and the downstream plume indicates that this enrichment does not originate from the main jet structure but instead corresponds to

a secondary fuel packet released after the primary injection phase, consistent with delayed needle closure in the pinhole injector.

By T_{SOI} = 1500 μs, the PLIF map shows that this enriched pocket has convected downstream and broadened. The centerline profile correspondingly shifts its peak location to approximately 45–55 mm downstream, while the magnitude decreases due to turbulent mixing and entrainment with the surrounding gas.

The combined spatial maps and centerline profiles, therefore, reveal a two-stage evolution of the mixture: the primary injection produces a distributed plume that propagates downstream, while a delayed secondary release forms a concentrated fuel packet near the injector that subsequently convects downstream and gradually mixes with the surrounding gas.

Aerodynamically, the hollow-cone jet can generate a toroidal vortex structure during the transient development of the jet. After the end of the main injection, the induced recirculating flow associated with this vortex can temporarily trap residual hydrogen near the injector region and enhance local mixing within the jet core. When combined with secondary hydrogen release from actuator rebound and delayed needle closure, this recirculating motion can intensify local fuel accumulation near the nozzle, producing a transient fuel-rich region ($\Phi \geq 1.0$). As the flow continues to evolve, this enriched pocket convects downstream and gradually disperses, as observed in the mixture field by T_{SOI} = 1500 μs. Such injector-induced fluctuations and localized enrichment events are important in engine applications, since unintended late fuel release can modify mixture stratification and influence subsequent ignition and combustion phasing

4 Summary

This study characterized hydrogen jet formation using a combined PLIF–LIBS methodology supported by schlieren imaging. Schlieren images provide intuitive jet images, allowing the basic structure of the jet, such as penetration and width, to be observed with minimal image processing. However, there is a limitation in converting the schlieren image into a local equivalence ratio map, as it shows only the accumulated pressure gradient from the side. The laser measurement technique is crucial for mapping the local equivalence ratio of the hydrogen jet. Although the Acetone-PLIF image can visualize the cross-sectional structure of the hydrogen jet, it must be calibrated using additional data. Combining PLIF and LIBS data converted the qualitative PLIF images into quantitative images by using LIBS point measurements as a reference.

The results showed that hydrogen jets evolve from hollow-cone structures with lean cores to vortex-driven enrichment in the mid-stages and eventually to momentum-dominated axial plumes, with strong temporal stratification throughout. Injection duration also played a critical role, as short pulses yielded narrow, stable plumes, whereas longer injections generated broader, but unstable jets with sustained enrichment at the core. A minor after-injection event was observed. Although the additional injection was

not significant, the behavior should be monitored during engine research to prevent unwanted engine damage caused by post-injection at unrealized engine crank angles. Together, these findings emphasize that hydrogen mixture preparation is governed by the interplay of nozzle design, ambient density, and injection strategy, and that the combined PLIF–LIBS technique provides a powerful framework for quantitative mapping and CFD validation in engine-relevant conditions.

Declarations

Conflict of interest

The authors have no competing interests to declare that are relevant to the content of this article.

Funding

This work was supported by the Material and Component Technology Development Project-Development and performance evaluation of key materials and components for hydrogen injection and supply systems for MW-class internal combustion engines (RS-2024-00430800) and International Cooperation Program for Industrial Technology-Development of World-Class 11L Direct Injection Hydrogen Engine Technology for Heavy Duty Applications in Response to Carbon Neutrality and CO2 Regulations (P0028449) funded by the Ministry of Trade, Industry & Resource (MOTIR, Korea).

Author Contribution

J.J.K, Y.K., and H.Y. conducted the experiment, S.L. provided the intiative of research topic, M.B. prepared figures 2 and 3, J.J.K. and S.L. wrote the main manuscript. J.H. and C.B. supervised the research.

Data availability

The datasets generated and analyzed during the current study are available from the corresponding author on reasonable request.

Tables

Tables 1 is available in the Supplementary Files section.

References

1. White C, Steeper R, Lutz A (2006) The hydrogen-fueled internal combustion engine: a technical review. International Journal of Hydrogen Energy 31 (10):1292–1305.

2. Onorati A, Payri R, Vaglieco B, Agarwal A, Bae C, Bruneaux G, Canakci M, Gavaises M, Günthner M, Hasse C, Ko S, John K, Kong S, Moriyoshi Y, Novella R, Pesyridis A, Reitz R, Ryan T, Wagner R, Zhao H (2022) The role of hydrogen for future internal combustion engines. International Journal of Engine Research 23(4):529–540.
3. Ji W, Wang S (2010) Combustion and emissions performance of a hybrid hydrogen-gasoline engine at idle and lean conditions. International Journal of Hydrogen Energy 35(1):346–355.
4. Goyal H, Jones P, Bajwa A, Parsons D, Akehurst S, Davy M, Leach F, Esposito S (2024) Design trends and challenges in hydrogen direct injection (H2DI) internal combustion engines - A review. International Journal of Hydrogen Energy 86:1179–1194.
5. Park C, Kim Y, Oh S, Oh J, Choi Y, Baek H, Lee S, Lee K (2022) Effect of fuel injection timing and injection pressure on performance in a hydrogen direct injection engine. International Journal of Hydrogen Energy 47(50):21552–21564.
6. Sementa P, Vargas Antolini J, Tornatore C, Catapano F, Vaglieco B, Sanchez J (2022) Exploring the potentials of lean-burn hydrogen SI engine compared to methane operation. International Journal of Hydrogen Energy 47(59):25044–25056.
7. Mohammadi A, Shioji M, Nakai Y, Ishikura W, Tabo E (2007) Performance and combustion characteristics of a direct injection SI hydrogen engine. International Journal of Hydrogen Energy 32(2):296–304.
8. Lee S, Kim G, Bae C (2022) Effect of mixture formation mode on the combustion and emission characteristics in a hydrogen direct-injection engine under different load conditions. Applied Thermal Engineering 209:118276.
9. Zhao H (2012) Laser diagnostics and optical measurement techniques in internal combustion engines. SAE International.
10. Kim J, Lee S, Ki Y, Hwang J, Bae C (2025) Feasibility of helium and nitrogen as surrogate gases for hydrogen jet using planar laser-induced fluorescence in a constant volume chamber. International Journal of Hydrogen Energy 172:151218.
11. Salazar V, Kaiser S, Halter F (2009) Optimizing precision and accuracy of quantitative PLIF of acetone as a tracer for hydrogen fuel. SAE International Journal of Fuels and Lubricants 2(1):737–761.
12. Blotevogel T, Egermann J, Goldlücke J, Leipertz A, Hartmann M, Schenk M, Berckmüller M (2004) Developing planar laser-induced fluorescence for the investigation of the mixture formation process in hydrogen engines. SAE Technical Paper 2004-01-1408.
13. Ki Y, Yang H, Kim J, Lee S, Hwang J, Bae C (2025) Stratified hydrogen combustion with various mixing processes. International Journal of Hydrogen Energy 169:151170.
14. Shudo T, Oba S (2009) Mixture distribution measurement using laser induced breakdown spectroscopy in hydrogen direct injection stratified charge. International Journal of Hydrogen Energy 34(5):2488–2493.

15. Ki Y, Kim J, Lee S, Hwang J, Bae C (2024) Mixing measurement on hydrogen jet by LIBS under various injection strategies. Proceedings of the Combustion Institute 40(1):105767.
16. Kazmouz S, Haworth D, Lillo P, Sick V (2021) Large-eddy simulations of a stratified-charge direct-injection spark-ignition engine: Comparison with experiment and analysis of cycle-to-cycle variations. Proceedings of the Combustion Institute 38(4):5849–5857.
17. Dec J (2009) Advanced compression-ignition engines-understanding the in-cylinder processes. Proceedings of the Combustion Institute 32(2):2727–2742.
18. Smirnov N, Nikitin V (2014) Modeling and simulation of hydrogen combustion in engines. International Journal of Hydrogen Energy 39(2):1122–1136.
19. Alfonso-Olmos E, Keenoy T, Shekhtman D (2025) Parametric study of acetone excitation for use in flow diagnostics. Optics Continuum 4(3):675–686.

Figures

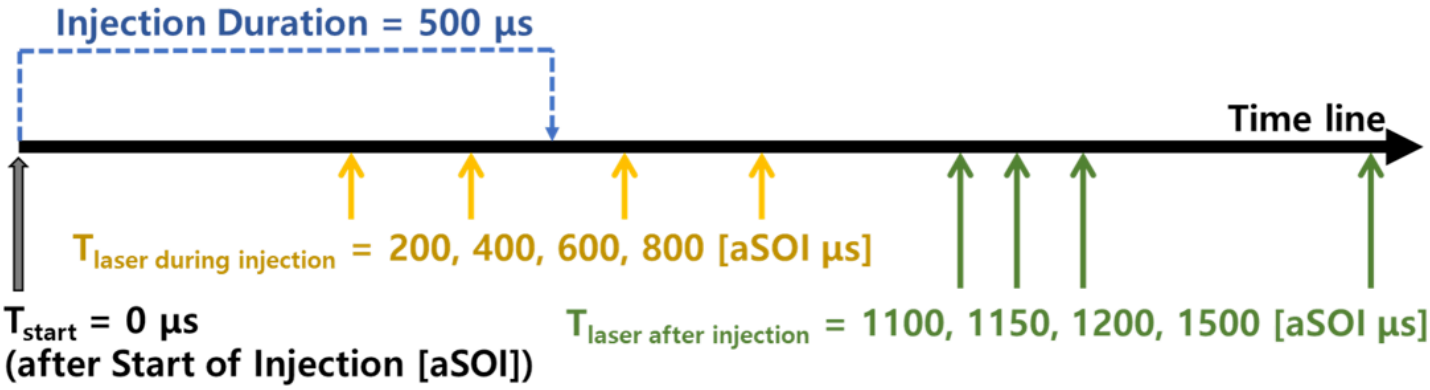


Fig. 1 Injection duration and laser timing during and after the injection are represented on a single timeline.

Figure 1

See image above for figure legend.

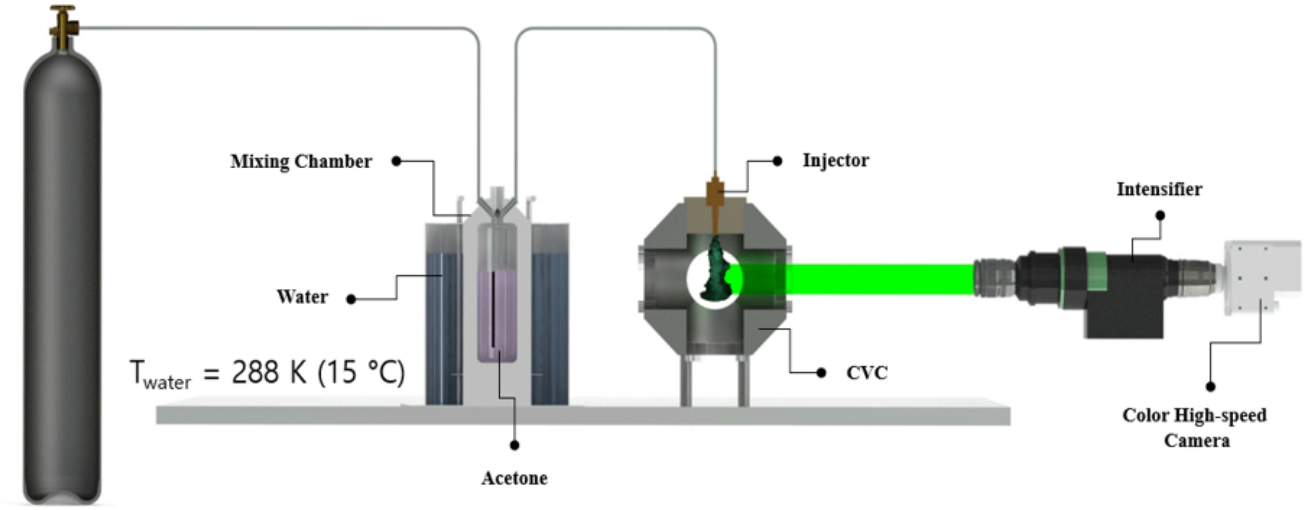


Fig. 2 Acetone and hydrogen mixture preparation chamber schematics with excitation and emission wavelength of acetone as PLIF tracer.

Figure 2

See image above for figure legend.

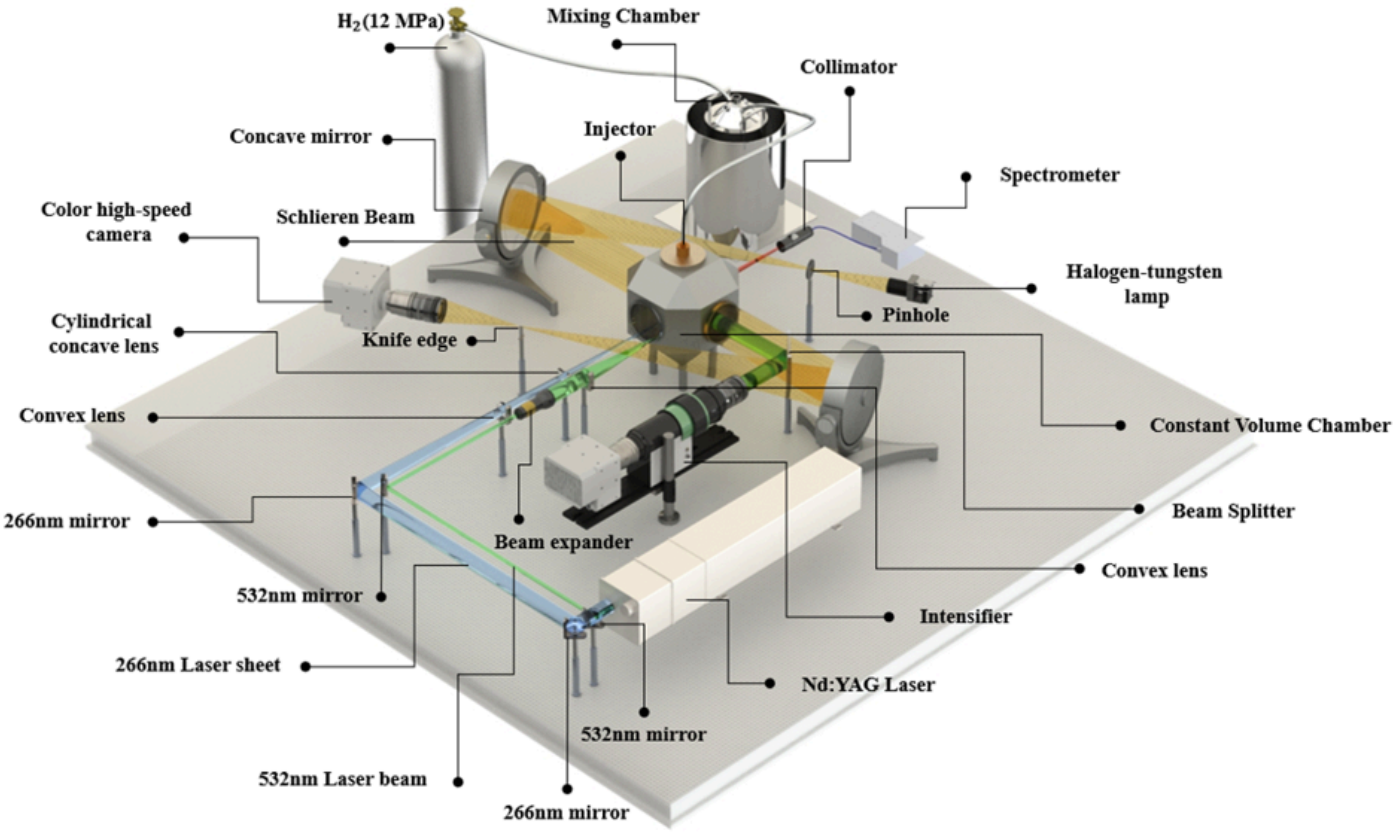


Fig. 3 Experiment setup for Planar Laser-induced Fluorescence and Laser-induced Breakdown Spectroscopy, including the optical setup and controllers.

Figure 3

See image above for figure legend.

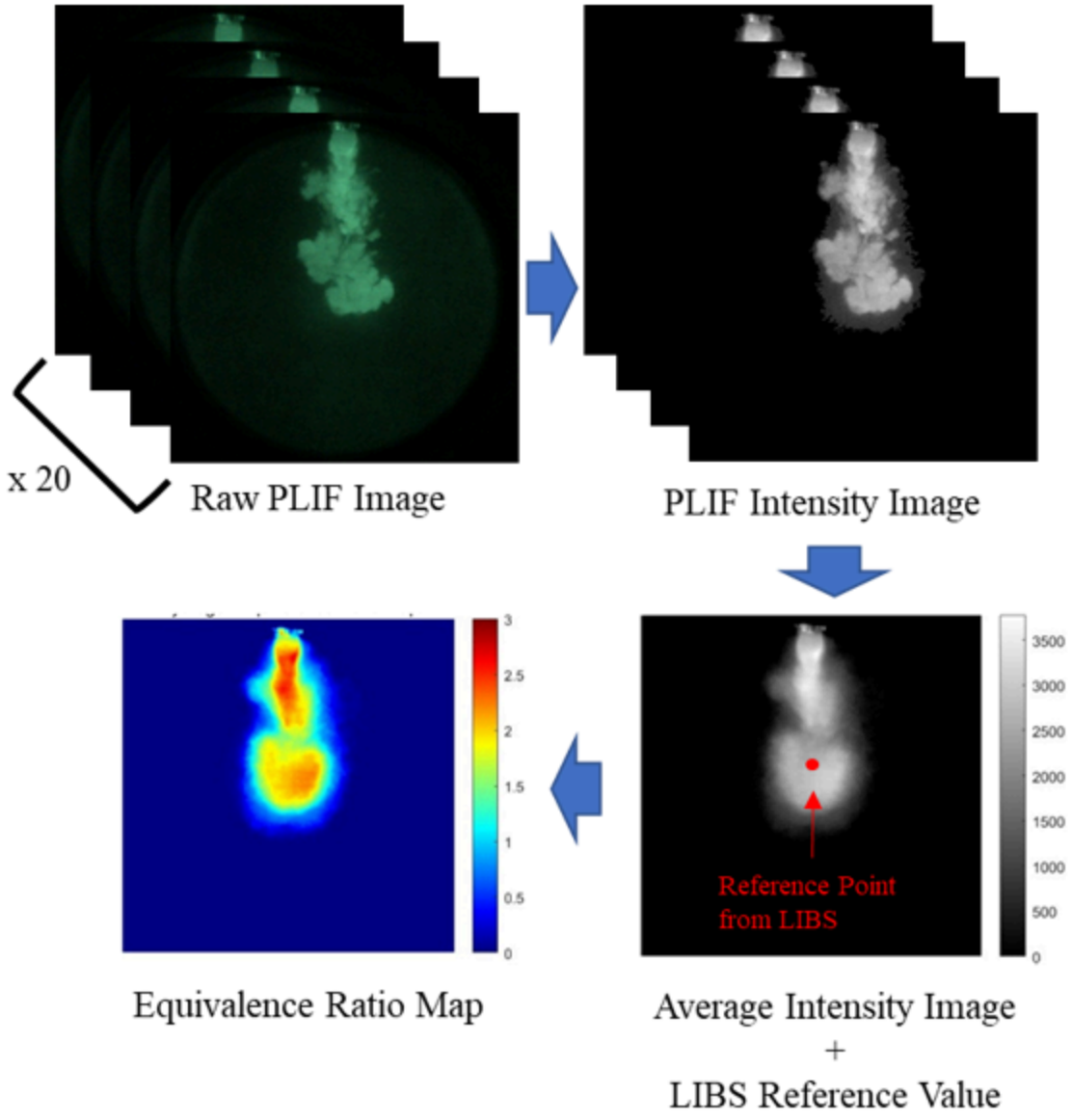


Fig. 4 PLIF and LIBS post-processing basic mechanism for each step from PLIF raw images (left-top) to hydrogen jet equivalence ratio map (left-bottom).

Figure 4

See image above for figure legend.

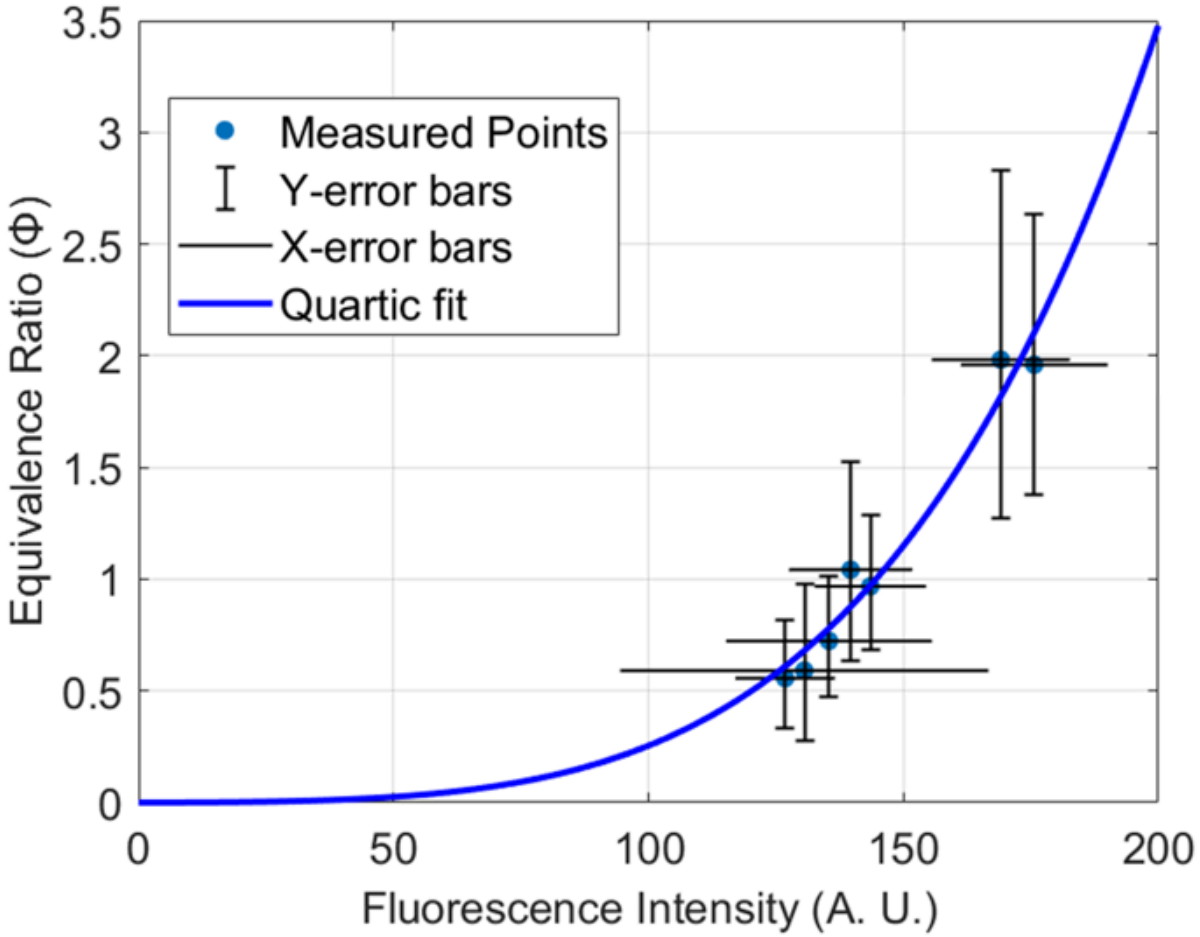


Fig. 5 Relationship between equivalence ratio (Y-axis) and fluorescence intensity (x-axis) represented as a quartic fit (blue line), including the error bars.

Figure 5

See image above for figure legend.

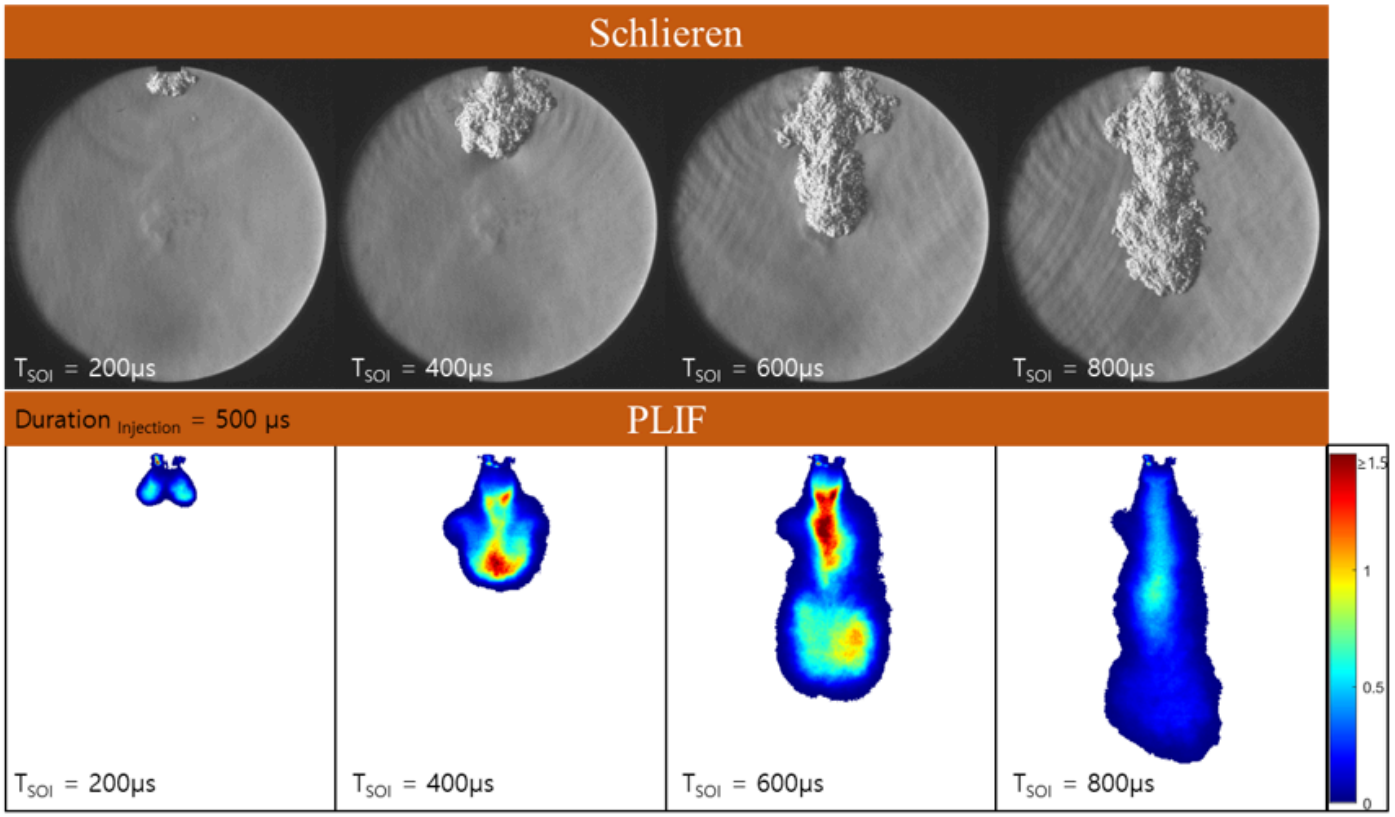


Fig. 6 Schlieren image (top) and post-processed equivalence ratio map (bottom) at the same moment from 200 μs after start of injection (left) to 800 μs after start of injection (right). The red area means that there is a rich hydrogen mixture, while the blue area represents a leaner mixture.

Figure 6

See image above for figure legend.

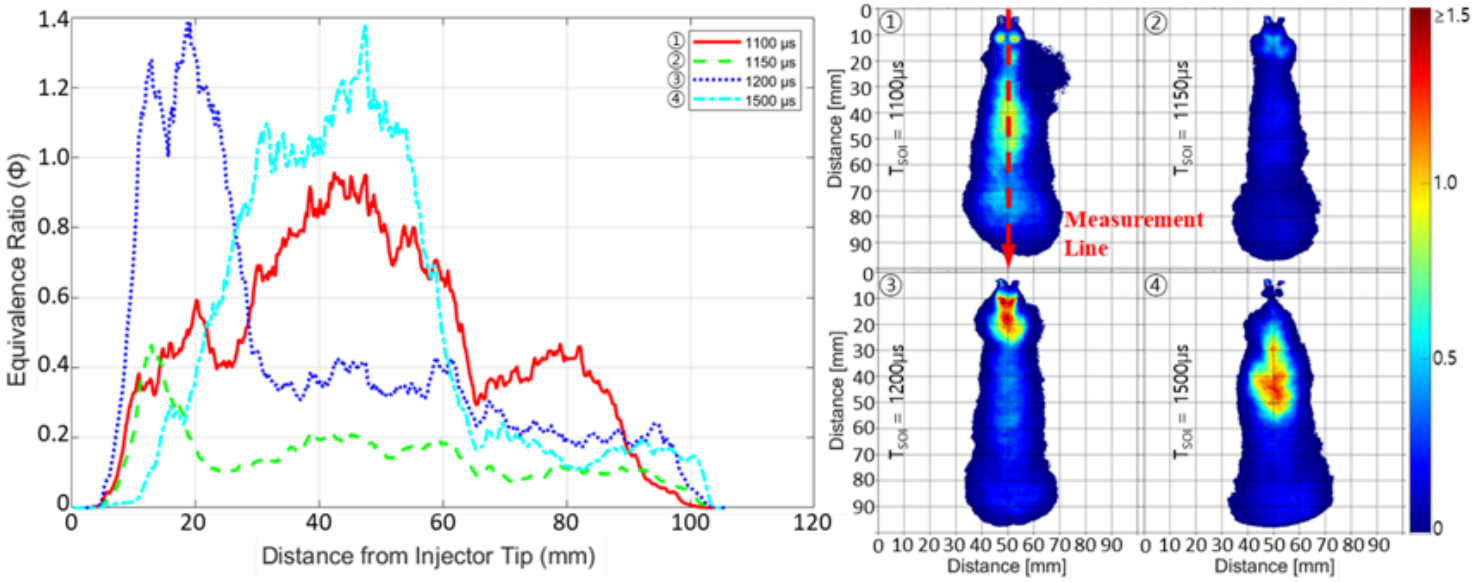


Fig. 7 Hydrogen jet equivalence ratio map between T_{SOI} = 1100 – 1500 μs (Left) and the measured equivalence ratio at the center of jet for each case (right)

Figure 7

See image above for figure legend.

Supplementary Files

This is a list of supplementary files associated with this preprint. Click to download.

- Tab.png